metals

MDPI

Article

Heterogeneous Nucleation Mechanisms in Systems with Large Lattice Misfit Demonstrated by the Pb(*l*)/Cu(*s*) System

Hua Men and Zhongyun Fan *

Brunel Centre for Advanced Solidification Technology (BCAST), Brunel University London, Uxbridge, Middlesex UB8 3PH, UK

* Correspondence: zhongyun.fan@brunel.ac.uk

Abstract: Our current understanding of heterogeneous nucleation has been largely confined to the classical nucleation theory (CNT) that was postulated over 100 years ago based on a thermodynamic approach. Further advances in heterogeneous nucleation research requires detailed knowledge of atomistic activities at the liquid/substrate interface. In this work, using a classical molecular dynamics (MD) simulation, we investigated the atomistic mechanisms of heterogeneous nucleation in systems with a large lattice misfit ($|f| > 12.5\%$) demonstrated by the liquid Pb and solid Cu system (denoted as the Pb(*l*)/Cu(*s*) system) with a misfit of 27.3%. We found that heterogeneous nucleation in systems with a large misfit takes place in two distinctive steps: (1) Prenucleation creates a coincidence site lattice (CSL) on the substrate surface to accommodate the majority (f_{csl}) of the initial misfit (f) and (2) Heterogeneous nucleation accommodates the residual misfit f_r (f_r = misfit − f_{csl}) at the nucleation temperature to create a plane of the new solid phase (a two-dimensional (2D) nucleus) through either a three-layer dislocation mechanism if $f_r < 0$ or a three-layer vacancy mechanism if $f_r > 0$, such as in the case of the Pb(*l*)/Cu(*s*) system.

Keywords: nucleation; atomistic simulation; solid/liquid interface; coincidence site lattice (CSL); lattice misfit

Citation: Men, H.; Fan, Z. Heterogeneous Nucleation Mechanisms in Systems with Large Lattice Misfit Demonstrated by the Pb(*l*)/Cu(*s*) System. *Metals* **2022**, *12*, 1583. https://doi.org/10.3390/met12101583

Academic Editor: Ayrat Nazarov

Received: 1 August 2022
Accepted: 19 September 2022
Published: 23 September 2022

1. Introduction

Based on the classical nucleation theory (CNT), Turnbull and Vonnegut [1] proposed a crystallographic model for a semi-coherent interface between the nucleus and the substrate, which suggests that nucleant potency (P) is inversely proportional to lattice misfit (f). They argued that this relationship might operate for many nucleation processes and suggested that there is a linear relationship between nucleation undercooling, ΔT_n, and misfit. However, Tóth et al. [2] pointed out that the barrier of heterogeneous nucleation was not a monotonical function of misfit, based on their modelling work with phase field crystal model. Interestingly, the recent experimental observations [3,4] showed that ΔT_n increased initially with increasing misfit, and reached a peak around misfit = 13%, and then decreased with further increase in misfit. It seems that the CNT not only breaks down for very potent particles [5], which usually have a very small lattice misfit with the new phase, but also does not work for the systems with a large misfit.

Atomistic simulation has been widely employed to understand the microscopic details of heterogeneous nucleation [6–13], due to the difficulties involved in experimental observations of the nucleation process [14]. With Monte Carlo simulations of crystal nucleation on a flat crystalline surface using the Lennard-Jones potential, Mithen et al. [13] found that the substrate surface lattice strongly influenced the nucleation rate, and the nucleation rate generally decreases with increasing misfit for misfit <10% and became scattered with further increase in misfit. They found that nucleation was epitaxial when misfit was small, and the epitaxy might be absent for systems with a large misfit [13].

Classical MD simulations for ice formation on kaolinite conducted by Sosso et al. [9] showed that the nucleus had a strong two-dimensional character, and that the critical nucleus was substantially smaller than that found for homogeneous nucleation. In addition, with ab initio MD simulations for the liquid Al/TiB_2 interface, Wang et al. [6] revealed that the growth of α-Al of three atomic layers in thickness at the interface was frustrated by the lattice misfit (f = −4.2%) between solid Al and TiB_2 at a small undercooling of 2 K. Furthermore, Fujinaga et al. [12] reported that a thin solid Al layer, which initially appeared in the liquid Al on surfaces of a cubic Ti particle, could grow to a spherical cap of fcc Al under an undercooling of 60 K, which was regarded as athermal heterogeneous nucleation by the authors. It seems that there has been an increasing interest in understanding of the atomistic mechanisms of heterogeneous nucleation process using atomistic simulations, and that the CNT has been commonly used as a framework to understand the simulation results [15–18] although discrepancies between the simulation results and the theoretical predictions by the CNT have been found in ice nucleation (as reviewed in [19]) and in other liquids [20–22]. So far, the exact atomistic mechanisms during the nucleation are still desirable.

The recent research works [6,14,23–33] have confirmed the existence of atomic ordering in the liquid adjacent to a crystalline substrate, which has been referred to as prenucleation that has a significant implication on the subsequent heterogeneous nucleation process. Based on these findings, the epitaxial model [34] proposed that structural templating might be the atomistic mechanism for heterogeneous nucleation, i.e., new phase continues the lattice of the substrate with creation of misfit dislocation at the interface to accommodate the lattice misfit. It predicts that the nucleation undercooling (ΔT_n) with increasing misfit in systems with the misfit of less than 12.5%, which is the theoretical upper limit for dislocation mechanism without overlapping of dislocation cores [34]. This implies that microscopic details of the structural templating may change with increasing the lattice misfit beyond 12.5%.

Lattice misfit (f) is defined as $f = (d_s - d_n)/d_s$, where d_s and d_n are the atomic spacing of the solid and the substrate, respectively [27]. Using MD simulations, Fan and Hua [35,36] systematically investigated the effect of lattice misfit on the atomistic mechanism of heterogeneous nucleation while the magnitude of misfit was less than 12.5%. They demonstrated that the heterogeneous nucleation completed deterministically within three atomic layers through structural templating to form a two-dimensional (2D) nucleus from which the new phase could grow, and this mechanism was referred to as three-layer nucleation [35,36]. For systems with a small negative misfit (−12.5% < misfit < 0), an edge dislocation network forms in the first layer to accommodate lattice misfit, a screw dislocation network forms in the second layer to reduce the lattice distortion caused by the edge dislocation network, and a perfect crystalline plane of the solid is created in the third layer as the 2D nucleus to template further growth [35]. They found that the potency of the substrate as measured by $1/\Delta T_n$ increased with the decrease in misfit, and this was in accordance with the prediction of the epitaxial model [34]. They also investigated the atomistic nucleation mechanism for systems with a small positive misfit (f < 12.5%) and found that the three-layer nucleation mechanism also worked for systems with a small positive misfit but with a different mechanism for accommodating the misfit [36]: the first layer is epitaxial to the substrate surface, the second layer contains vacancies to accommodate lattice misfit, and the third layer is the 2D nucleus that templates further growth. However, the atomistic mechanism of heterogeneous nucleation for systems with a large misfit (f > 12.5%) is yet to be investigated.

The Pb(l)/Cu(s) system has a large positive misfit (27.3%) and is immiscible at the melting temperature of Pb thus there exists a 'clean' interface between liquid Pb and (111) Cu substrate [8,23]. In addition, the potentials for the Pb(l)/Cu(s) system have been developed by Hoyt et al. [37] and tested widely for their reliability in simulating the Pb/Cu system [8,23,38,39]. Therefore, it provides a unique model system to investigate the atomistic nucleation mechanisms in systems with a large misfit. Using the classical MD

simulations, Palafox-Hernandez et al. [23] observed the 2–3 "prefreezing" layers of crystalline Pb at the liquid Pb/solid (111) Cu interface at 625 K and such atomic ordering in the liquid at temperatures above the liquidus was generally referred to as prenucleation [27]. Palafox-Hernandez et al. [8] later showed that at a ΔT_n of 26 K the nucleation and growth of Pb on the Cu substrate occurred primarily layer-wise, without formation of the hemispherical cap. It seems that the ΔT_n of the Pb(l)/Cu(s) system is considerably small, compared to 130 K for the systems with misfit = ±8% under similar simulation conditions reported in the literature [35,36]. It is in qualitative agreement with experimental results that the system with a larger misfit may exhibit a lower ΔT_n while misfit is larger than 13% [3]. In fact, the experiment for the nucleation of Pb droplet in Cu matrix revealed that the (111) Cu was very potent for nucleating solid Pb, with a measured ΔT_n being 0.5 K and measured θ being 4° [40], where the CNT broke down [40]. However, it is still not clear how such a large lattice misfit is accommodated at the Pb(l)/Cu(s) interface during nucleation, and what is the atomistic mechanism for heterogeneous nucleation in the systems with a large lattice misfit.

In this study, we investigated both prenucleation and heterogeneous nucleation processes in the systems with a large lattice misfit, using the classical MD simulation. For this purpose, the Pb/Cu system was taken as an example. The objective of this study is to capture the fundamental information about evolution of the atomic arrangements at the stage of prenucleation and the atomistic mechanism of heterogeneous nucleation for the systems with a large lattice misfit.

2. Simulation Approach

We used the embedded-atom method (EAM) potentials for the Cu-Pb interatomic interactions, developed by Hoyt et al. [37]. The melting temperatures calculated with the potentials are 1279 K for Cu [37] and 618 K for Pb [23,41], compared to the experimental values of 1357.8 K for Cu and 600.6 K for Pb [42]. The parallel MD program LAMMPS [43] (12 Dec 2018 version, Sandia National Laboratories, Sandia, NM, USA) was used for the MD simulations. The simulation system consists of the liquid Pb (Pb(l), hereafter) and the solid Cu (Cu(s), hereafter) with a <111> surface orientation, with the z axis being normal to the {111} Cu, which has been confirmed experimentally to be the nucleating surface [40]. The dimensions of the Cu(s) are $96[11\bar{2}] \times 60[\bar{1}10] \times 18[111]$, and the initial dimensions of the Pb sample are $69[11\bar{2}] \times 42[\bar{1}10] \times 27[111]$, with a total atom number of 30321. The apparent lattice misfit between the solid Pb and Cu is misfit = 27.3% at 618 K, and the details of the calculation of misfit can be found in Ref. [27]. The Cu(s) is either partially or fully relaxed. For the former, the atoms in the innermost layer of the Cu are fixed to avoid Brownian motion in the Cu(s) and the others can move freely [23]. For the latter, all atoms in the Cu(s) can move freely while the "fix recentre" command in the LAMMPS is implemented to constrain the centre-of-mass of Cu(s). Periodic boundary conditions are imposed in the $x([11\bar{2}])$- and $y([\bar{1}10])$-directions of all the systems, and a vacuum region is inserted with periodic boundary conditions in the z([111])- direction, with the extent of 60 Å.

The equations of motion were integrated by means of the Verlet algorithm with a time step of 0.001 ps, and the Berendsen NVT ensemble was used for the temperature control. The initial systems were heated to a temperature of 700 K with a step of 50 K, each lasting 100,000 MD steps. The system equilibrated at 700 K was taken as the initial configuration and cooled to the desired temperature firstly with a temperature step of 5 K. At each temperature step, the system could run for 1,000,000 MD steps to equilibrate, and the variation in the total energy and the trajectory of the system were monitored until the nucleation was observed, at which the temperature of T was denoted as T_{5K}. The system equilibrated at T_{5K} + 5 K was taken as a new initial configuration and cooled to the desired temperature with a step of 1 K until the nucleation event was observed, and this temperature was referred to as the nucleation temperature, T_n. We found that both the systems

with partially and fully relaxed substrates exhibited essentially the same behaviour during the nucleation.

The atomic ordering at the interface is characterized by atomic density profile, $\rho(z)$ [28], and z-dependent in-plane order parameter, $S(z)$ [44], where z is the distance away from the interface. The details for calculating $\rho(z)$ and $S(z)$ can be found in Ref. [27].

Stress profile, σ_s (z), measures the difference between the longitudinal and transverse diagonal components of the pressure (stress) tensor, and can be expressed as [23]:

$$\sigma_s(z) = P_{zz} - 1/2\ [P_{xx}(z) + P_{yy}(z)] \quad (1)$$

where P_{ij} is the component of the pressure tensor. To obtain $\sigma_s(z)$, the local stress tensor associated with individual atomic positions and the Voronoi tessellation of the atoms were calculated, using the procedure implemented in LAMMPS [45].

The time-averaged atomic positions and the local bond-order analysis are employed to investigate the atomic arrangement in the Pb at the interface. To perform the local bond-order analysis, the local bond-order parameters, $\boldsymbol{q}_l(i)$, is calculated: [46]

$$\boldsymbol{q}_l(i) = \left(\frac{4\pi}{2l+1}\sum_{m=-l}^{l}|\boldsymbol{q}_{lm}(i)|^2\right)^{1/2} \quad (2)$$

where the $(2l + 1)$ dimensional complex vector $\boldsymbol{q}_{lm}(i)$ is the sum of spherical harmonics, $Y_{lm}(r_{ij})$, over all the nearest neighbouring atoms of the atom i. Two neighbouring atoms i and j can be recognised to be connected if the correlation function, $\boldsymbol{q}_6(i) \cdot \boldsymbol{q}_6(j)$, exceeds a threshold of 0.5. An atom is identified as solid if the number of the connections that this atom has with its neighbours reaches a threshold of 6.

3. Results

3.1. Prenucleation

Figure 1a is a snapshot of the Pb(l)/Cu(s) system equilibrated at 625 K. The liquid Pb atoms adjacent to the Pb(l)/Cu(s) interface become layered despite the existence of a large lattice misfit (27.3%). The quantified density profile, $\rho(z)$, as a function of distance, z, is plotted in Figure 1b, where $z = 0$ marks the Gibbs dividing interface. It is noted in Figure 1b that the atomic density profile has a smooth transition from the bulk liquid Pb to the solid Cu across the Pb(l)/Cu(s) interface. There are three transitional Cu(s) layers and six transitional Pb(l) layers at the interface. This density profile is typical of the systems with an atomically flat substrate surface and with either a positive [36] or negative [35] lattice misfit, supporting the previous conclusion that atomic layering at the liquid/substrate interface is independent of lattice misfit as long as the substrate surface is flat.

Time-averaged atomic positions were used to investigate the atomic arrangements at the Pb(l)/Cu(s) interface. Figure 2 shows the time-averaged atomic positions of the first Cu(s) layer (denoted as L1Cu) and the CSL Pb layer (CSL) and the first (L1Pb), second (L2Pb), and third (L3Pb) layers of Pb(l) in the Pb(l)/Cu(s) system equilibrated at 625 K, where the CSL represents coincidence site lattice (CSL, we will discuss it in detail later). Firstly, we observed neither Cu atoms in liquid Pb layers nor Pb atoms in solid Cu layers at the Pb(l)/Cu(s) interface at 625 K although a few Cu solute atoms in the liquid Pb at the interface were found during the simulation at 700 K. This confirms the MD simulation results obtained by Palafox-Hernandez et al., [23], being consistent with the fact that Cu-Pb is an immiscible system. Secondly, we noticed that the completely ordered Cu surface layer (L1Cu) in Figure 2a templated two completely ordered layers in liquid Pb adjacent to the Pb(l)/Cu(s) interface, CSL (Figure 2b) and L1Pb (Figure 2c). Finally, further away from the interface atomic ordering decreases quickly to that of the liquid Pb (Figure 2d,e).

The layered structures at the Pb(l)/Cu(s) interface equilibrated at 625 K are subjected to further quantitative analysis and the results are presented in Figure 3. The quantified peak density, ρ_p, is shown in Figure 3a. There are three Cu layers adjacent to the interface that have a decreased peak density compared with that of the bulk Cu, while there are six

liquid Pb layers showing an exponential decay of peak density away from the interface (Figures 1b and 3a).

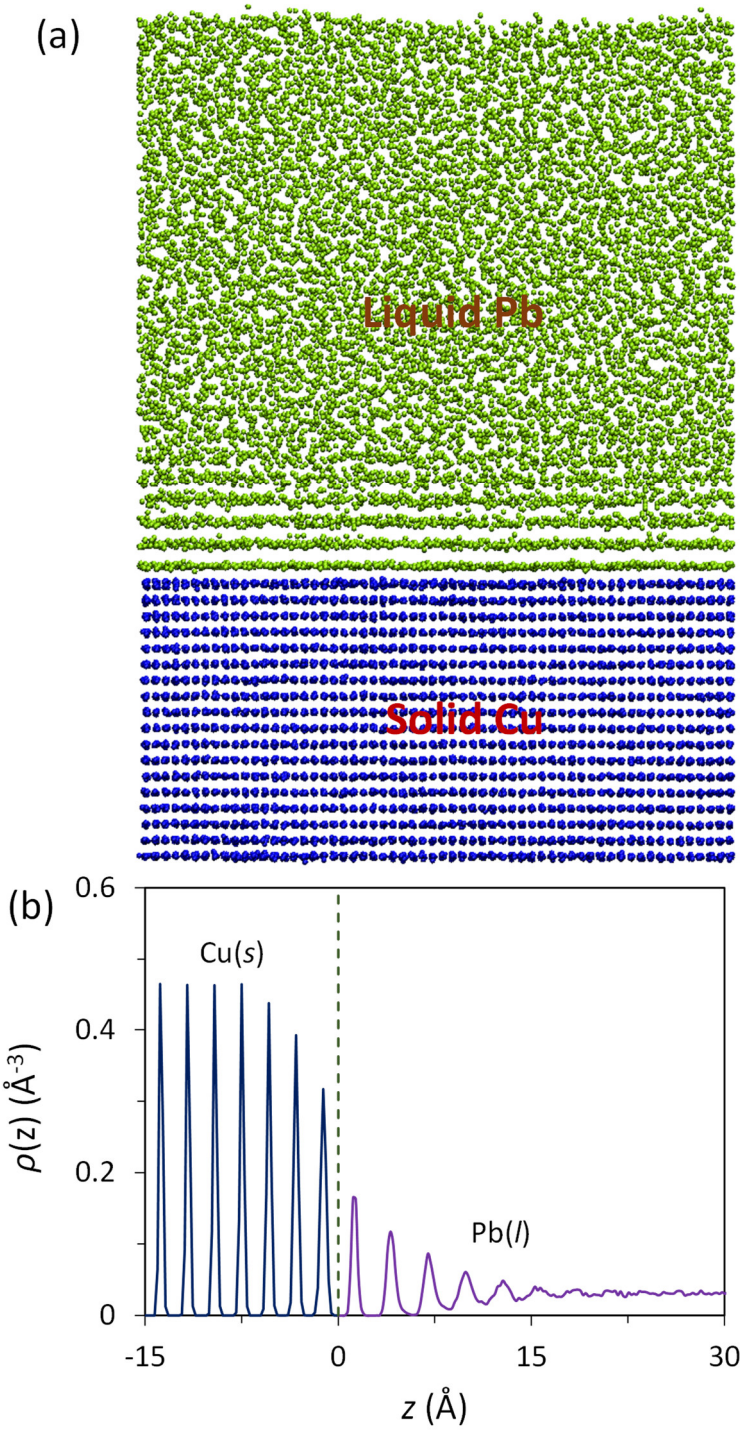

Figure 1. Prenucleation phenomenon in the Pb(*l*)/Cu(*s*) system equilibrated at 625 K. (**a**) Snapshot (front view) of the system and (**b**) atomic density profile, $\rho(z)$, as a function of distance, z, from the interface. The dashed line at $z = 0$ in (**b**) marks the Pb(*l*)/Cu(*s*) interface. Liquid Pb adjacent to the liquid/substrate interface shows 6 distinctive atomic layers.

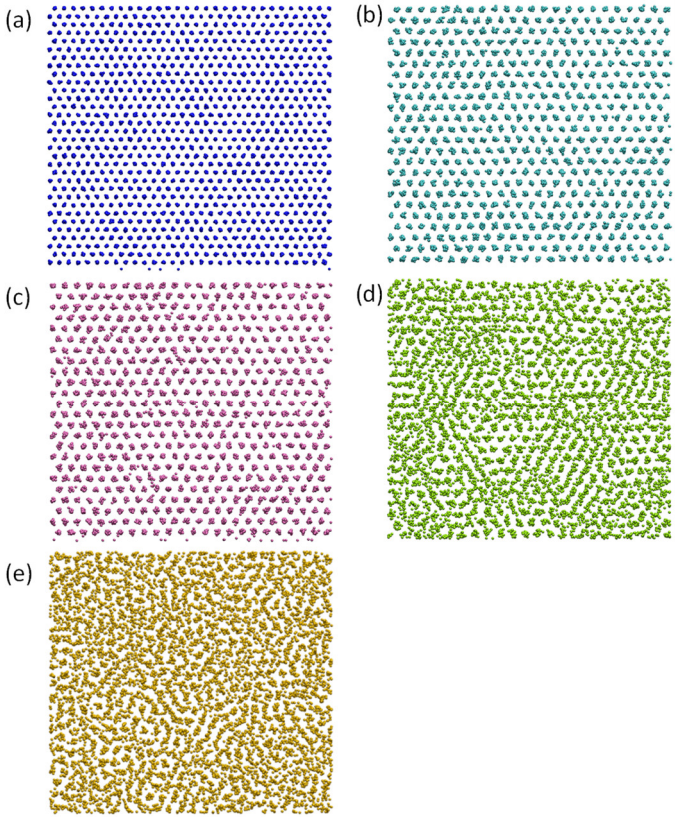

Figure 2. Time-averaged atomic positions showing the atomic arrangement in the Pb(*l*)/Cu(*s*) system equilibrated at 625 K (above the melting temperature of Pb (618 K)). (**a**) First Cu layer (L1Cu); (**b**) the CSL Pb layer (CSL, coincidence site lattice); (**c**) the 1st (L1Pb), (**d**) 2nd (L2Pb) and (**e**) 3rd (L3Pb) layers of Pb at the interface. These results suggest that there exists a 2D ordered structure in the liquid Pb induced by the Cu substrate.

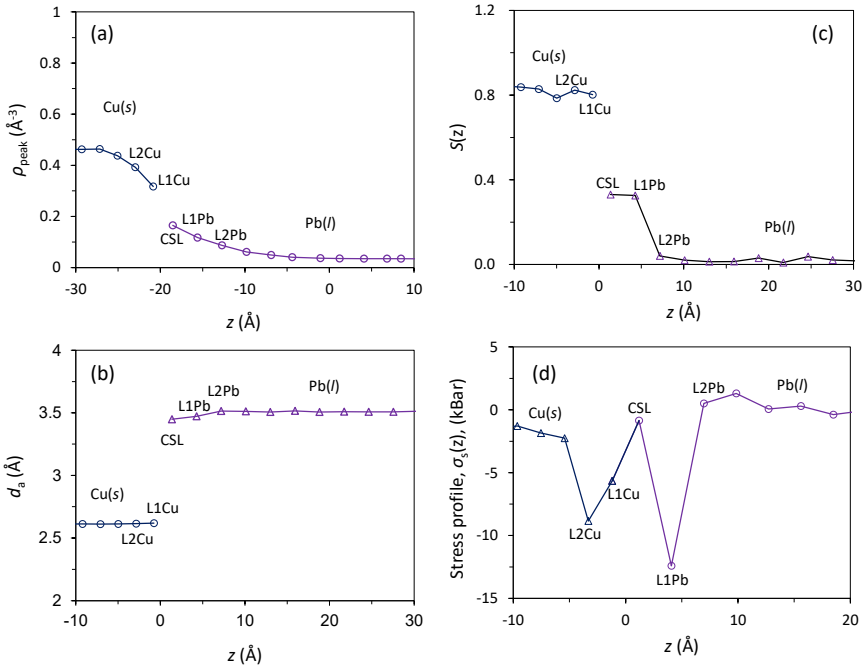

Figure 3. Characteristics of the 2D ordered structures in liquid Pb adjacent to the Pb(*l*)/Cu(*s*) interface equilibrated at 625 K; (**a**) peak density, $\rho_P(z)$; (**b**) in-plane order parameter, $S(z)$; (**c**) average in-plane atomic spacing, d_a; and (**d**) local stress distribution, $\sigma_s(z)$, are plotted as a function of the distance, z, from the interface.

The in-plane order parameter, $S(z)$, for the Pb(l)/Cu(s) system equilibrated at 625 K is displayed in Figure 3b as a function of distance from the interface. While the $S(z)$ values for the solid Cu are consistently high (around 0.8), only the CSL and L1 layers for the liquid Pb have relatively high $S(z)$ values (around 0.4) and $S(z)$ value is approaching zero further away from the interface. Figures 2 and 3b suggest that there exists a 2D ordered structure within 2–3 atomic layers at the interface. Compared with the systems with a small lattice misfit ($|f| < 12.5\%$), it is noted that pronounced atomic ordering exists in the Pb(l)/Cu(s) system with a large misfit ($f = 27.3\%$). This is referred to as prenucleation [27].

The atomic spacing, d_a, in the individual layer is obtained by averaging the distances between all the nearest neighbouring atoms in this layer and is plotted as a function of z for the Pb(l)/Cu(s) systems equilibrated at 625 K in Figure 3c. It is interesting to note that the atomic spacings for the CSL and L1 layers are slightly smaller than that of the bulk liquid Pb but almost identical to the bulk solid Pb ($d_a = 3.53$ Å). The time-averaged atomic positions (Figure 2b,c), the quantified $S(z)$ (Figure 3b), and the average atomic spacing d_a (Figure 3c) suggest that the CSL and L1 layers are completely ordered.

The quantified stress profile, $\sigma_s(z)$, is presented in Figure 3d as a function of distance from the interface for the system equilibrated at 625 K. Figure 3d reveals the following facts: (1) The stress levels in the bulk liquid Pb and bulk solid Cu are close to zero, indicating that the Pb(l)/Cu(s) system at 625 K is in equilibrium; (2) The "w" shaped stress profile suggests that the atoms in CSL layer is stress free, L1Pb, L1Cu and L2Cu are in compression; (3) The "w" shaped stress profile is in good agreement with the result of Palafox-Hernandez et al. [23].

To sum up, at temperatures close to but above the liquidus of Pb (618 K), there exists prenucleation in the systems with a large lattice misfit: the substrate induces a 2D ordered structure within 2–3 atomic layers at the interface.

3.2. Coincidence Site Lattice (CSL)

We have investigated the detailed atomic arrangements in CSL Pb layer relative to that in the substrate surface (L1Cu). Figure 4a shows the time-averaged atomic positions of CSL Pb layer superimposed on that of L1Cu layer in the Pb(l)/Cu(s) system equilibrated at 625 K. The atoms in Figure 4a exhibit a regular hexagonal pattern, which is too fine to be an edge dislocation network as observed in the systems with a small negative misfit [35]. Further analysis reveals that the relationship between CSL Pb and L1Cu can be best described by a coincidence site lattice (CSL), as demonstrated by the snapshot in Figure 4b and illustrated by the unit cells in Figure 4c. This CSL can be described by the orientation relationship between CSL Pb and L1Cu: (111)<110>Pb // (111)<110>Cu, and $3d_{Pb<110>} = 4d_{Cu<110>}$ matching of atomic spacings along the <110> directions of both Pb and Cu. This is equivalent to the low energy Σ7 CSL existing in the grain boundary [47]. According to this atomic matching rule, the lattice misfit accommodated by the CSL is calculated to be 25% (denoted as f_{csl}), which accounts for a major part of the initial lattice misfit (27.3%) between CSL Pb and L1Cu layers.

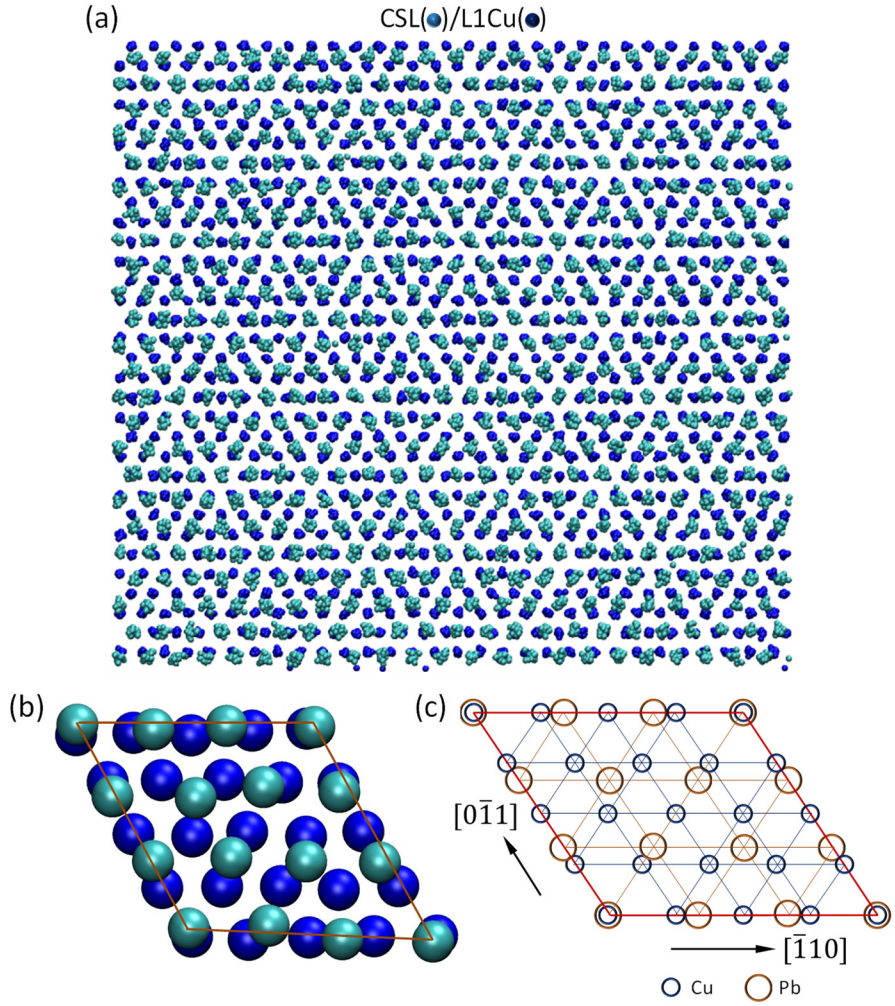

Figure 4. Formation of coincidence site lattice (CSL) during prenucleation in the Pb(*l*)/Cu(*s*) system equilibrated at 625 K; (**a**) time-averaged atomic positions (top view) of CSL Pb layer superimposed on that of L1Cu; (**b**) snapshot of CSL/L1Cu showing the atomic arrangement in the CSL unit cell; (**c**) schematic illustration of CSL unit cell showing the matching rule, $3d_{Pb} = 4d_{Cu}$, where d is the atomic spacing along the <011> direction.

The lattice misfit between the consecutive layers, f_a, at the interface is calculated using the following equation:

$$f_a = \left[\frac{d_2 - d_1}{d_2}\right] \times 100\% \quad (3)$$

where d_2 and d_1 are atomic spacing of a given atomic layer and that of its underneath layer, respectively. Figure 5 shows the f_a as a function of z for the Pb(*l*)/Cu(*s*) system equilibrated at 625 K. The calculated f_a between the CSL Pb and L1Cu is 24%, which is close to the theoretical value of 25% lattice misfit that the Σ7 CSL can accommodate. In addition, Figure 5 suggests that L1Pb accommodates 0% lattice misfit.

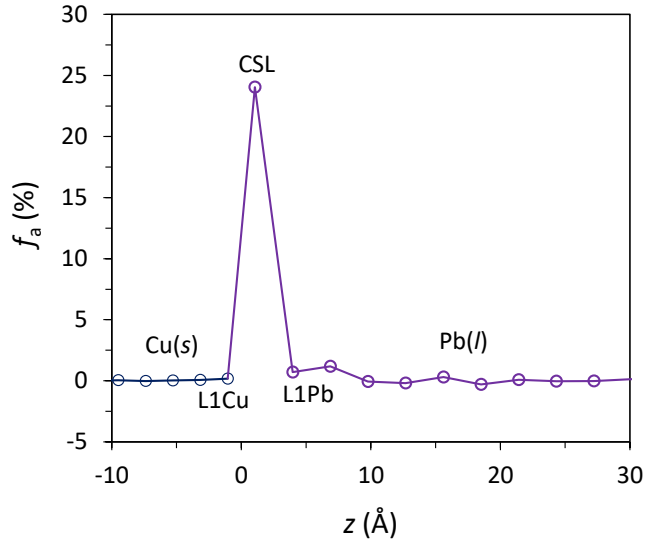

Figure 5. The accommodated misfit, f_a, of the individual layer as a function of distance (z) from the interface during prenucleation in the Pb(l)/Cu(s) system equilibrated at 625 K.

3.3. Heterogeneous Nucleation

The nucleation temperature, T_n, was determined to be 594 K for the Pb(l)/Cu(s) system by monitoring the total energy of the simulation system using the approaches described in Section 2. The nucleation undercooling, ΔT_n, is expressed as: $\Delta T_n = T_m - T_n$, where T_m is 618 K for the Pb [37]. Thus, ΔT_n is 24 K, being in good agreement with the value of 26 K obtained by Palafox-Hernandez et al. [8].

The 2D ordered structure in the liquid Pb adjacent to the liquid/substrate interface at the onset of nucleation (t = 0 ps) represents the maximum atomic ordering in the liquid Pb achievable by prenucleation and is referred to as the precursor of heterogeneous nucleation. Figure 6 shows the atomic arrangement in the precursor. The time-averaged atomic positions of the CSL-L3Pb at t = 0 ps during the simulation at T_n = 594 K are presented in Figure 6a–d. Both CSL Pb (Figure 6a) and L1Pb (Figure 6b) have an ordered structure, while L2Pb (Figure 6c) and L3Pb (Figure 6d) contain some ordered regions in a liquid matrix. Compared with the 2D ordered structure at 625 K (Figure 2), the precursor contains more ordered atoms. The layering of Pb at the interface increases slightly from six layers at 625 K (Figure 1b) to seven at T_n (Figure 6e). In addition, both the peak density, $\rho_P(z)$ (Figure 6f), and the in-plane order parameter, $S(z)$ (Figure 6g), have increased slightly compared with those at 625 K. This is consistent with our previous observation [27] that the atomic ordering of the liquid at the interface increases with decreasing the temperature.

We firstly analysed qualitatively the evolution of atomic ordering in the interfacial Pb layers during the nucleation process using time-averaged atomic positions. The onset of nucleation is marked by an increase in atomic ordering in the liquid adjacent to the interface during isothermal holding at the nucleation temperature. The evolution of atomic ordering is clearly revealed by the time-averaged atomic positions in the first four Pb layers (CSL-L3Pb) at the interface at different times during the nucleation process at T_n = 594 K. In the precursor (t = 0 ps, Figure 6a–d), CSL Pb and L1Pb are largely ordered structure while L2Pb and L3Pb are considerably disordered. Atomic ordering in L2Pb and L3Pb increases with time, and L3Pb is transformed into a complete crystalline plane at t = 190 ps. L3Pb has a hexagonal atomic arrangement and atomic spacing (d_a = 3.53 Å) matching that of the {111}Pb plane (d_a = 3.53 Å) of the bulk Pb at T_n = 594 K. Here we define L3Pb as the 2D nucleus, which marks the end of nucleation and onset of crystal growth. Thus, in the case of the Pb(l)/Cu(s) system, t < 0 ps is prenucleation with the precursor as an

outcome; 0 ps ≤ t ≤ 190 ps is the nucleation process and the nucleus is a 2D plane of the solid phase; and t > 190 ps is crystal growth.

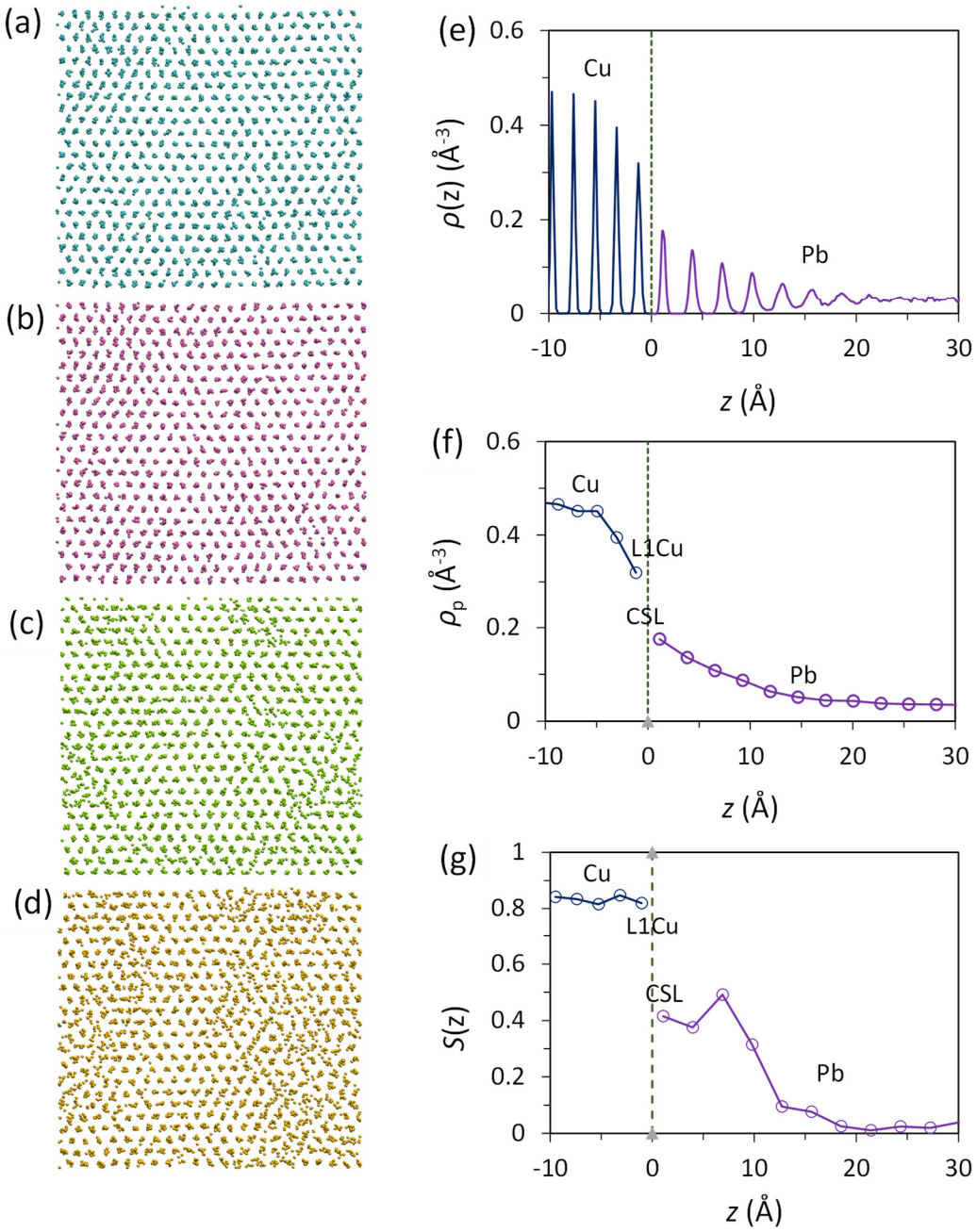

Figure 6. Nucleation precursor represents the maximum atomic ordering in the liquid adjacent to the interface prior to the onset of nucleation. Time-averaged atomic positions of (**a**) CSL, (**b**) L1Pb, (**c**) L2Pb and (**d**) L3Pb. (**e**) Density profile, $\rho(z)$; (**f**) peak density, $\rho_P(z)$; and (**g**) in-plane atomic ordering, $S(z)$, are plotted as a function of distance z from the interface for the Pb(l)/Cu(s) system at t = 0 ps during the simulation at T_n = 594 K.

We then analysed quantitatively the atomic ordering during nucleation by quantifying the evolution of peak density, $\rho_P(z)$, and the fraction of solid atoms, f_s, at T_n = 594 K as functions of time (t) and distance from the interface represented by atomic layers, and the results were presented in Figure 7. Before the onset of nucleation (t < 0 ps), the atomic ordering in the system has the following characteristics: (1) the peak density profile is independent of time as shown by the overlapping peak density profiles at t = −150 ps and

t = 0 ps in Figure 7a; (2) the fraction of solid atoms, f_s, has a constant value (independent of time) for a specific Pb layer (Figure 7b); and (3) f_s is 1 for CSL Pb and close to 1 for L1Pb suggesting the CSL Pb and L1Pb become completely ordered at prenucleation stage (Figure 7b). All these suggests that the atomic ordering at the nucleation temperature is constant before the onset of nucleation although it is dynamic with time. During nucleation (0 ps ≤ t ≤ 190 ps), the peak density profile rises (Figure 7a) and the fraction of solid atoms increases (Figure 7b) with increasing time until $\rho_p(z)$ reaches the peak density for solid Pb and f_s reach 1 for L3Pb. Crystal growth (t > 190 ps) is characterised by advancing the Pb(s)/Pb(l) interface with a flat "z" shaped peak density profile into the liquid away from the substrate (Figure 7a) and repeating the flat "s" shaped f_s curves to create further solid layers (Figure 7b). The general observation from Figure 7 is that the increase in atomic ordering is considerably slower during nucleation than that during subsequent crystal growth.

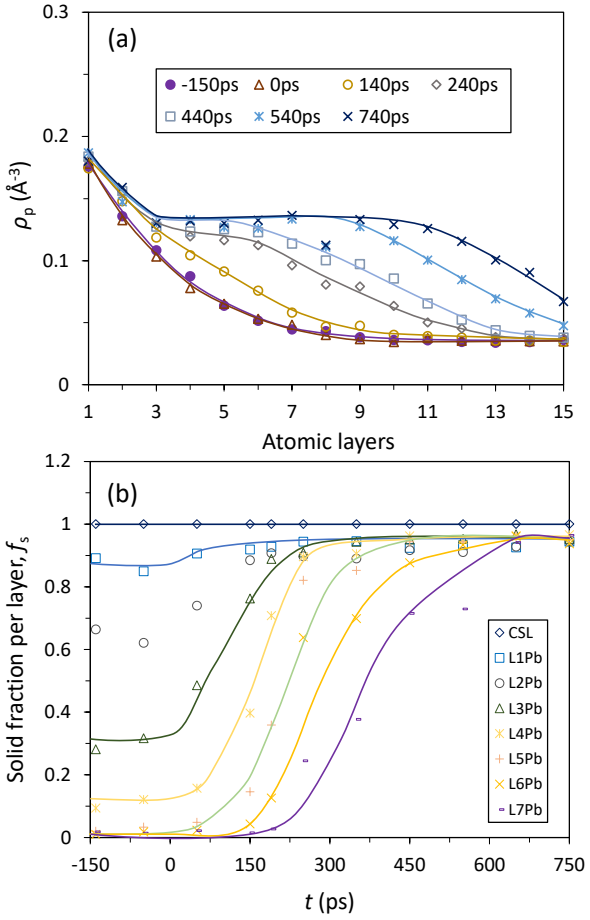

Figure 7. Evolution of atomic ordering during heterogeneous nucleation in the Pb(l)/Cu(s) system at T_n = 594 K; (**a**) Peak density, $\rho_p(z)$, and (**b**) solid fraction, $f_s(z)$, of the individual Pb layers at the interface are plotted as functions of t and the atomic layer away from the interface.

The results in Figure 7 suggest that both heterogeneous nucleation and crystal growth in the Pb(l)/Cu(s) system proceed layer-by-layer through a structural templating mechanism, in which ordered atoms in a given atomic layer provide low energy positions for the ordered atoms in the next neighbouring layer. This means that along the z direction, a solid atom always "sits" on top of solid atoms in its underneath layer.

The detailed atomic arrangement of Pb at the end of nucleation (t = 190 ps) is further analysed. Figure 8a shows the time-averaged atomic positions of CSL Pb layer superimposed on top of that of L1Cu. Analysing the regular patterns in Figure 8a reveals the exact

same coincidence site lattice (CSL) as shown in Figure 4. This suggests that the ordered CSL layer forms at the prenucleation stage and should be treated as part of the substrate as long as the heterogeneous nucleation is concerned. Figure 8b shows the time-averaged atomic positions of L1Pb superimposed on top of that of CSL Pb layer. It is interesting to note that (1) All the Pb atoms in L1Pb (in red) sit above the centre of the upward triangles formed by Pb atoms in CSL Pb layer (in light blue) (Figure 8b); (2) L1Pb contains no vacancies (f_v = 0 % in Figure 9a); and (3) L1Pb has almost the same average atomic spacing (d_a = 3.45 Å) as that of CSL Pb layer (Figure 9b). All these suggest that L1Pb is in an epitaxial relationship with CSL Pb layer. Figure 8c displays a snapshot of L2Pb at t = 190 ps. Different from the epitaxial L1Pb, L2Pb contains 4.3% vacancies (Figure 9a) and has a slightly higher atomic spacing (d_a = 3.53 Å, Figure 9b).

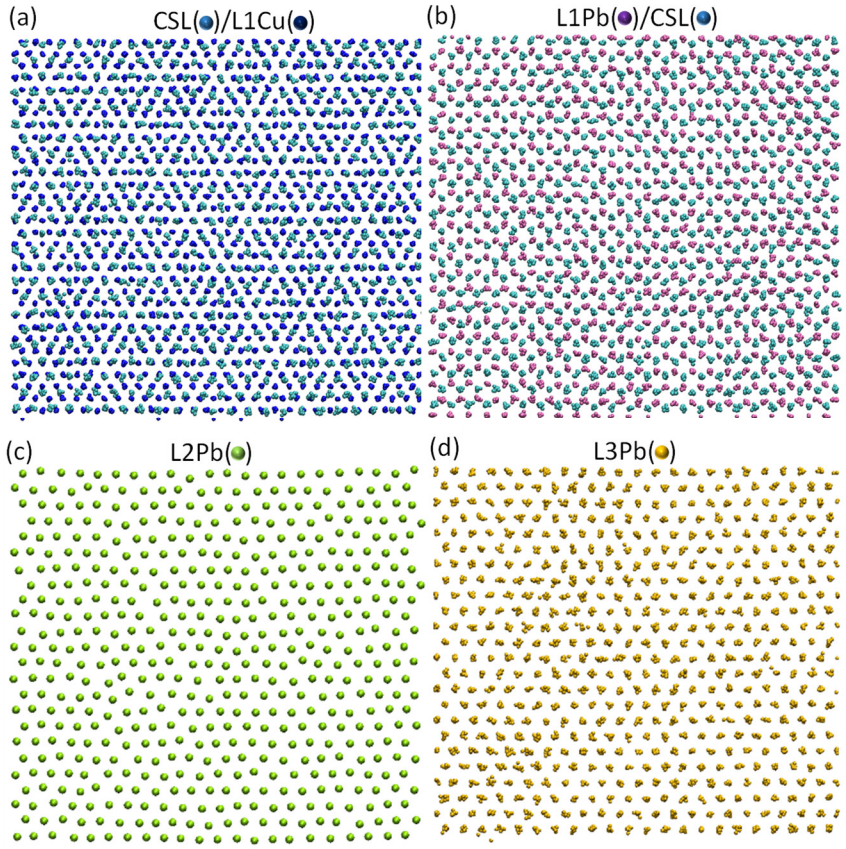

Figure 8. Atomic arrangements in the Pb(*l*)/Cu(*s*) system at T_n = 594 K at the end of nucleation (t = 190 ps); (**a**) Time-averaged atomic positions of CSL Pb/L1Cu showing coincidence site lattice (CSL) as a mechanism to accommodate the major lattice misfit; (**b**) time-averaged atomic positions of L2Pb/CSL Pb showing the epitaxial relationship between L1Pb and CSL Pb; (**c**) a snapshot of L2Pb showing the existence of vacancies (as quantified in Figure 9a) as a mechanism to accommodate the residual lattice misfit; and (**d**) time-averaged atomic positions of L3Pb showing a perfect plane of (111) Pb as a 2D nucleus that demarcates the end of nucleation and the start of crystal growth.

Figure 8d presents the time-averaged atomic positions of L3Pb at t = 190 ps. Detailed analysis confirmed that L3Pb contained only a small fraction of vacancies that was comparable with equilibrium vacancy concentration, but no other defects were found. In addition, L3Pb (Figure 8d) has a hexagonal atomic arrangement and an average atomic spacing of d_a = 3.53 Å, which matches well those of (111) plane of the bulk solid Pb. Therefore, L3Pb can be taken as a 2D nucleus, which marks the end of heterogeneous nucleation and the onset of crystal growth.

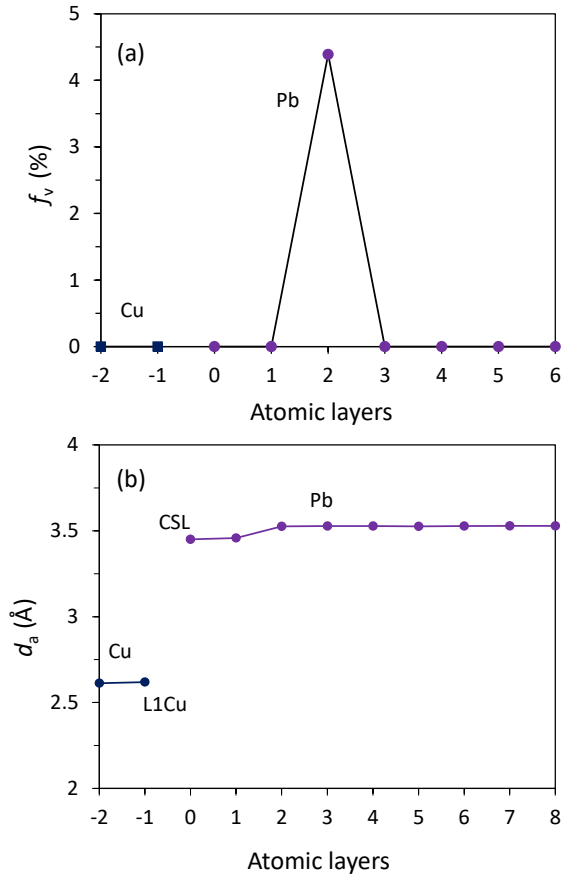

Figure 9. The (**a**) vacancy concentration, f_v, and (**b**) average in-plane atomic spacing, d_a, of the individual Pb layers at the interface as a function of the distance, z, from the interface for the Pb(l)/Cu(s) system at T_n = 594 K and t = 1000 ps.

4. Discussion

In this study, we have investigated the atomistic mechanisms of heterogeneous nucleation in systems with a large lattice misfit (f > 12.5%) through MD simulations using the Pb(l)/Cu(s) system (27.3% misfit) as an example. We find that prenucleation at temperatures above the liquidus of Pb produces a completely ordered solid layer, which has a CSL relationship with the {111} Cu surface and accommodates 25% lattice misfit. The CSL is best described by the following orientation relationship (OR) and atomic matching rule (AMR):

$$(111)\langle 110\rangle \text{Pb} \,//\, (111)\langle 110\rangle \text{Cu}, \quad \text{(OR 1)} \tag{4}$$

$$3d_{\text{Pb}\langle 110\rangle} = 4d_{\text{Cu}\langle 110\rangle} \qquad \text{(AMR1)} \tag{5}$$

The CSL layer can be treated as a new surface layer and induces a 2D ordered structure in the liquid Pb, which acts as a precursor for heterogeneous nucleation at the nucleation temperature. Building on the precursor, heterogeneous nucleation takes place through a three-layer mechanism: The first Pb layer has an epitaxial relationship with the CSL Pb layer; the second Pb layer contains vacancies to accommodate the residual lattice misfit (2.3%); and the third Pb layer is a perfect {111} Pb plane, which acts as a 2D nucleus to template further growth. This three-layer mechanism is the same as that for heterogeneous nucleation in the systems with a small positive misfit (0 < misfit < 12.5%) [36]. Therefore, the mechanisms for heterogeneous nucleation in the Pb(l)/Cu(s) system (27.3% misfit) can be described by two distinctive steps. Step 1: formation of CSL Pb layer as a new substrate surface at the stage of prenucleation to accommodate most of the lattice misfit (25%), which transforms the system from one with a large misfit to another with a small

residual lattice misfit (2.3%); step 2: a three-layer mechanism to generate a 2D nucleus. In this section, we discuss the generality of this mechanism for heterogeneous nucleation for systems with a large misfit.

Nucleation potency can be measured by the nucleation undercooling, ΔT_n. Our MD simulation suggests that the nucleation undercooling of the Pb(*l*)/Cu(*s*) system is 24 K. This is in accordance with ΔT_n = 26 K in the study of the same system by Palafox-Hernandez et al. [8], and in qualitative agreement with the experimentally measured ΔT_n (0.5 K) for the nucleation of the solid Pb in a liquid droplet contained in the solid Cu matrix by Kim and Cantor [40], considering the large differences in solidification conditions between the experiment and the MD simulation. Now let us put the nucleation undercooling of the Pb(*l*)/Cu(*s*) system into a wider context of nucleation undercooling as a function of lattice misfit. Figure 10 shows a comparison of the nucleation undercooling of the Pb(*l*)/Cu(*s*) system with that for the Pb(*l*)/Al(*s*) system [48] and for the generic liquid/substrate systems with a small lattice misfit [35,36]. By ignoring the effect of chemical interaction, Figure 10 suggests that (1) nucleation undercooling increases with increasing the absolute value of lattice misfit $|f|$ for a small misfit regardless of its sign (positive or negative); (2) nucleation undercooling is not a monotonic function of lattice misfit, as has been suggested previously by Fan [34], Granasy et al. [2] and confirmed by experimental observations [3,4]; (3) the nucleation undercooling for system with a large misfit is comparable with that for systems with a small misfit if the residual misfit (f_r) after CSL formation is used for comparison. This may be attributed to the fact that CSL has a small contribution to the interfacial energy [47], and CSL has little effect on the nucleation undercooling.

Now let us generalise the atomistic mechanisms for heterogeneous nucleation as a function of lattice misfit. Figure 11 illustrates schematically the nucleation undercooling and nucleation mechanisms for systems with different lattice misfit, where misfit denotes the initial lattice misfit calculated from atomic spacings, f_{csl} is the lattice misfit accommodated by CSL during prenucleation, f_r is the residual lattice misfit after formation of CSL, which needs to be accommodated during heterogeneous nucleation at the nucleation temperature. It is obvious that the following relationship exists between these parameters:

$$f = f_{csl} + f_r. \quad (6)$$

Here we provide a summary of the heterogeneous nucleation mechanisms for systems with various lattice misfit assuming that the substrate surface is atomically flat and that there is no chemical interaction between the substrate and the liquid:

- For the systems with misfit = 0%, the nucleation undercooling will be zero if there are no considerations for chemical interaction between the liquid and the substrate and the surface roughness of the substrate.
- For the systems with a small negative misfit (−12.5% < misfit < 0), heterogeneous nucleation takes place through a three-layer dislocation mechanism [35]: formation of an edge dislocation network to accommodate lattice misfit in the first layer; formation of a screw dislocation network to reduce lattice distortion in the second layer resulting in a twist of the new crystal relative to the substrate; and creation of a plane of the new solid (the third layer) as a 2D nucleus.
- For the systems with a small positive misfit (12.5% > misfit > 0), heterogeneous nucleation takes place through a three-layer vacancy mechanism [36]: formation of an epitaxial layer to the substrate surface in the first layer; formation of vacancies to accommodate lattice misfit in the second layer; and creation of a plane of the new solid (the third layer) as a 2D nucleus.
- For the systems with a large misfit ($|f|$ > 12.5%), formation of CSL during prenucleation accommodates most of the lattice misfit (f_{csl}) and converts the system from one with a large misfit to another with a small misfit ($|f_r|$ < 12.5%); heterogeneous nucleation takes place through a three-layer mechanism at the nucleation temperature: a three-layer dislocation mechanism if the residual lattice misfit is less than 0; a three-layer vacancy mechanism if the residual lattice misfit is larger than 0.

The exact mechanism of heterogeneous nucleation for systems with a large misfit depends on the sign of residual lattice misfit (f_r) rather than the sign of the initial misfit (f). The sign of f_r can be either positive or negative for systems with both a negative and positive misfit since $|f_{csl}|$ can be larger than $|f|$.

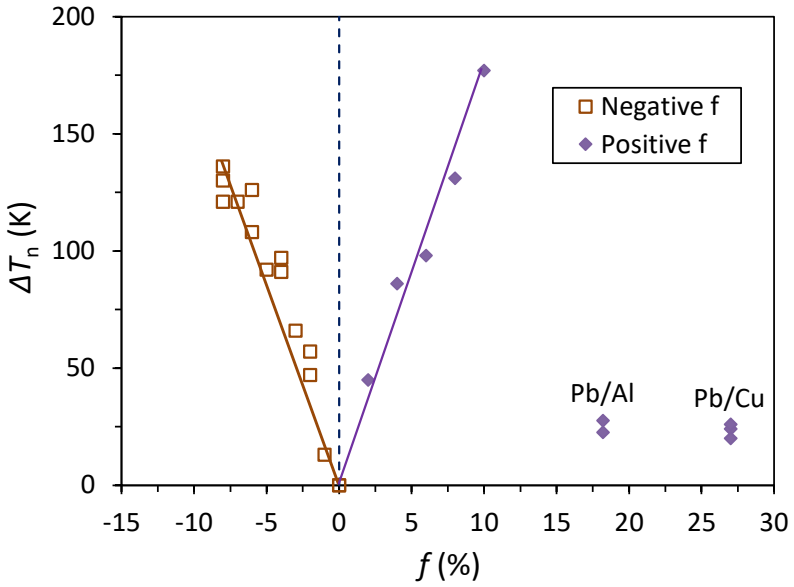

Figure 10. Nucleation undercooling (ΔT_n) obtained by MD simulations as a function of lattice misfit (f) [49]. The data points for the Pb(l)/Cu(s) system (as labelled) are from this work, and those for the Pb(l)/Al(s) system (as labelled) are from Ref. [48] and the rest of data points are from Refs. [35,36].

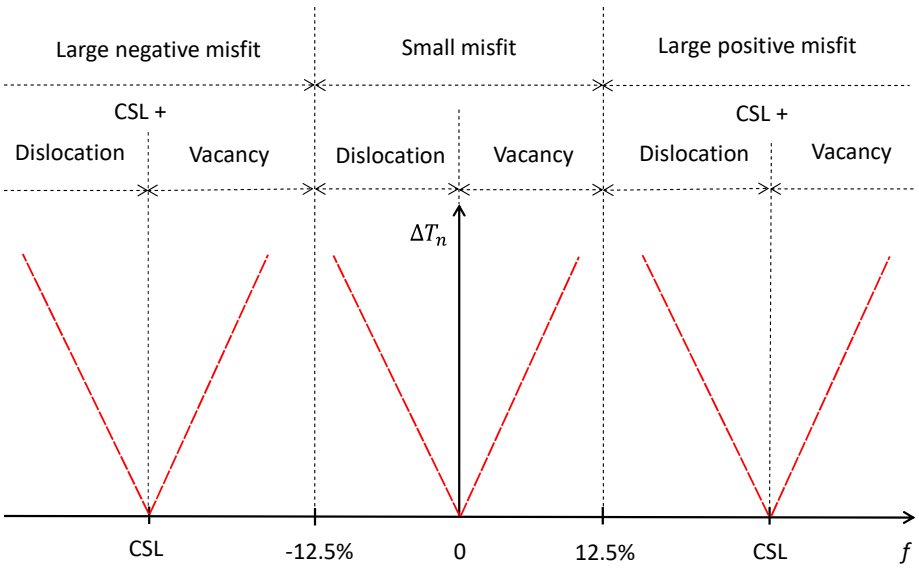

Figure 11. Schematic illustration of mechanisms for accommodating lattice misfit and nucleation undercooling (ΔT_n) as a function of lattice misfit (f). For systems with a small negative misfit (0 > misfit > −12.5%), nucleation takes place through a 3-layer dislocation mechanism; for systems with a small positive misfit (0 < misfit < 12.5%), nucleation takes place through a 3-layer vacancy mechanism; for systems with a large misfit ($|f|$ > 12.5%), nucleation takes place by two distinctive steps: (1) prenucleation creates CSL to accommodate the majority of the misfit (f_{csl}); and (2) heterogeneous nucleation at the nucleation temperature to create a 2D nucleus through either a 3-layer dislocation mechanism if the residual lattice misfit is less than 0 or a 3-layer vacancy mechanism if the residual lattice misfit is larger than 0.

It is important to point out that the nucleation mechanisms presented in Figure 11, particularly those for systems with negative residual misfit (($f_r < 0$), are speculations (or extrapolations) based on the current MD simulations, and further work is required to confirm the validity of such mechanisms.

A major insight from this study is that the coincidence site lattice (CSL) is an effective mechanism to accommodate lattice misfit during prenucleation for the systems with a large lattice misfit. Formation of CSL transforms a system with a large lattice misfit into one with a small residual misfit, and hence extends the three-layer mechanisms for heterogeneous nucleation into systems with a large misfit. As has been extensively studied in the grain boundary [50], CSLs usually have relatively small interfacial energy, and are described by the Σ notation, which is defined as the ratio of atom numbers in the unit cells of two grains (or planes) [47]. However, for describing heterogeneous nucleation, where structural templating becomes critically important [34], we suggest that CSL is described by a specific orientation relationship (OR) between the two planes and two independent atomic matching rules (AMRs):

$$(hkl)[uvw]_{sol} // (h'k'l')[u'v'w']_{sub}, \text{ (OR 2)} \quad (7)$$

$$m_1 d_{sol1} = n_1 d_{sub1}, \text{ (AMR2)} \quad (8)$$

$$m_2 d_{sol2} = n_2 d_{sub2}, \text{ (AMR3)} \quad (9)$$

where "$_{sol}$" denotes the solid, "$_{sub}$" the substrate, "$_1$" matching direction 1, "$_2$" matching direction 2, and m and n are integral numbers. From these matching directions lattice misfit can be calculated from the relevant atomic spacings. It is obvious that in the case of the Pb(l)/Cu(s) system, the two matching directions are equivalent directions (<110>), and the two matching rules are the same.

In this study, heterogeneous nucleation is defined as the process of creating isothermally a 2D nucleus at T_n, which is a crystal plane of the new solid. As has been described in our previous studies [35,36], this 2D nucleation process is spontaneous (barrierless) and deterministic at the nucleation temperature. This is obviously different from the CNT, which describes the heterogeneous nucleation as a cap formation process (i.e., the creation of a 3D nucleus) through fluctuation of local atomic structures, compositions, and temperature [51]. As suggested previously, the cap formation process in the CNT is better described as grain initiation process, which is deterministically dependent on the substrate size [52]. After creation of the 2D nucleus, solidification enters the growth stage. Further crystal growth may need to overcome an energy barrier before free growth depending on the substrate size [52,53].

5. Summary

In this paper, we investigated the atomistic mechanisms of both prenucleation and heterogeneous nucleation in the systems with a large lattice misfit using molecular dynamics (MD) simulations. The liquid Pb/solid Cu (denoted as Pb(l)/Cu(s)) provides a unique example for the systems with a large positive misfit since: (1) it has a lattice misfit of 27.3% between the solid Pb and the Cu substrate; (2) it has well developed and tested potentials; and (3) it is an immiscible system at the melting point of Pb avoiding the complication with formation of solid solutions. We find that at the stage of prenucleation, a coincidence site lattice (CSL) forms between the CSL layer of Pb and surface layer of Cu substrate at the interface and accommodates the majority (f_{csl} = 25%) of the initial misfit (f) in the system. The CSL transforms the original Cu substrate with a large misfit into one with a small residual misfit (f_r = misfit − f_{csl}, and f_r = 2.3% in this case). At an undercooling of 24 K, heterogeneous nucleation proceeds layer-by-layer: The L1Pb layer is epitaxial to the CSL Pb layer; the L2Pb Layer contains vacancies to accommodate the residual misfit; and the L3Pb layer is a perfect plane of the solid Pb (the 2D nucleus) that templates further growth of the solid Pb. This is the same three-layer vacancy mechanism we reported previously for the systems with a small positive misfit. Here we propose that for systems

with a large misfit ($|f| > 12.5\%$), heterogeneous nucleation takes place in two distinctive steps: (1) formation of CSL to accommodate most of the misfit (f_{csl}) at the stage of prenucleation and (2) heterogeneous nucleation at the nucleation temperature to create a 2D nucleus through either a three-layer dislocation mechanism if the residual misfit is less than 0 or a three-layer vacancy mechanism if the residual misfit is larger than >0.

Author Contributions: H.M. conducted classical MD simulations and visualization, and original draft writing; Z.F. conducted conceptualization of the research, funding acquisition, and supervision. All authors have read and agreed to the published version of the manuscript.

Funding: This work has been funded by the EPSRC of the UKRI under the grant number EP/N007638/1.

Institutional Review Board Statement: Not applicable.

Informed Consent Statement: Not applicable.

Data Availability Statement: All data is available in the main text.

Acknowledgments: The authors like to thank Wang, Y.; Gao F. for constructive suggestions and manuscript reading.

Conflicts of Interest: The authors declare no conflicts of interest.

References

1. Turnbull, D.; Vonnegut, B. Nucleation catalysis. *Ind. Eng. Chem*. **1952**, *44*, 1292–1298.
2. Tóth, G.I.; Tegze, G.; Pusztai, T.; Gránásy, L. Heterogeneous crystal nucleation: The effect of lattice mismatch. *Phys. Rev. Lett*. **2012**, *108*, 025502.
3. Wang, L.; Yang, L.; Zhang, D.; Xia, M.; Wang, Y.; Li, J.G. The role of lattice misfit on heterogeneous nucleation of pure aluminium. *Metall. Mater. Trans. A* **2016**, *47*, 5012–5022.
4. Wang, L.; Lu, W.Q.; Hu, Q.D.; Xia, M.X.; Wang, Y.; Li, J.G. Interfacial tuning for the nucleation of liquid AlCu alloy. *Acta Mater*. **2017**, *139*, 75–85.
5. Cantor, B. Heterogeneous nucleation and adsorption. *Phil. Trans. R. Soc. Lond. A* **2003**, *361*, 409–417.
6. Wang, J.S.; Horsfield, A.; Schwingenschlögl, U.; Lee, P.D. Heterogeneous nucleation of solid Al from the melt by Al_3Ti: Molecular dynamics simulations. *Phys. Rev. B* **2010**, *82*, 184203.
7. Wearing, D.; Horsfield, A.P.; Xu, W.W.; Lee, P.D. Which wets TiB_2 inoculant particles: Al or Al_3Ti? *J. Alloys Compd*. **2016**, *664*, 460–468.
8. Palafox-Hernandez, J.P.; Laird, B.B. Orientation dependence of heterogeneous nucleation at the Cu-Pb solid-liquid interface. *J. Chem. Phys*. **2016**, *145*, 211914.
9. Sosso, G.C.; Li, T.S.; Donadio, D.; Tribello, G.A.; Michaelides, A. Microscopic mechanism and kinetics of ice formation at complex interfaces: Zooming in on kaolinite. *J. Phys. Chem. Lett*. **2016**, *7*, 2350–2355.
10. Cabriolu, R.; Li, T.S. Ice nucleation on carbon surface supports the classical theory for heterogeneous nucleation. *Phys. Rev. E* **2015**, *91*, 052402.
11. Lin, H.H.; Li, T.; Li, H. Molecular dynamics study on the heterogeneous nucleation of liquid Al-Cu alloys on different kinds of copper substrates. *Phys. Chem. Chem. Phys*. **2018**, *20*, 29856–29865.
12. Fujinaga, T.; Shibuta, Y. Molecular dynamics simulation of athermal heterogeneous nucleation of solidification. *Comput. Mater. Sci*. **2019**, *164*, 74–81.
13. Mithen, J.P.; Sear, R.P. Computer simulation of epitaxial nucleation of a crystal on a crystalline surface. *J. Chem. Phys*. **2014**, *140*, 084504.
14. Greer, A.L. Liquid metals: Supercool order. *Nat. Mater*. **2006**, *5*, 13–14.
15. Tipeev, A.O.; Zanotto, E.D.; Rino, J.P. Crystal nucleation kinetics in supercooled germanium: MD simulations versus experimental data. *J. Phys. Chem. B* **2020**, *124*, 7979–7988.
16. Tipeev, A.O.; Zanotto, E.D. Nucleation kinetics in supercooled $Ni_{50}Ti_{50}$: Computer simulation data corroborate the validity of the classical nucleation theory. *Chem. Phys. Lett*. **2019**, *735*, 136749.
17. Prado, S.C.C.; Rino, J.P.; Zanotto, E.D. Successful test of the classical nucleation theory by molecular dynamic simulations of BaS. *Comput. Mat. Sci*. **2019**, *161*, 99–106.
18. Tipeev, A.O.; Zanotto, E.D.; Rino, J.P. Diffusivity, interfacial free energy and crystal nucleation in a supercooled Lennard-Jones liquid. *J. Phys. Chem. C* **2018**, *122*, 28884–28894.
19. Sosso, G.C.; Chen, J.; Cox, S.J.; Fitzner, M.; Pedevilla, P.; Zen, A.; Michaelides, A. Crystal nucleation in liquids: Open questions and future challenges in molecular dynamics simulations. *Chem. Rev*. **2016**, *116*, 7078–7116.

20. Xia, X.S.; Van Hoesen, D.C.; McKenzie, M.E.; Youngman, R.E.; Kelton, K.F. Low-temperature nucleation anomaly in silicate glasses shown to be artifact in a $5BaO{\cdot}8SiO_2$ glass. *Nat. Commun.* **2021**, *12*, 2026.
21. Cassar, D.R.; Serra, A.H.; Peitl, O.; Zanotto, E.D. Critical assessment of the alleged failure of the Classical Nucleation Theory at low temperatures. *J. Non-Cryst. Solids* **2020**, *547*, 120297.
22. Fokin, V.M.; Zanotto, E.D.; Yuritsyn, N.S.; Schmelzer, J.W.P. Homogeneous crystal nucleation in silicate glasses: A 40 years perspective. *J. Non-Cryst. Solids* **2006**, *352*, 2681–2714.
23. Palafox-Hernandez, J.P.; Laird, B.B.; Asta, M. Atomistic characterization of the Cu-Pb solid-liquid interface. *Acta Mater.* **2011**, *59*, 3137–3144.
24. Kaplan, W.D.; Kauffmann, Y. Structural order in liquids induced by interfaces with crystals. *Annu. Rev. Mater. Res.* **2006**, *36*, 1–48.
25. Oh, S.H.; Scheu, C.; Rühle, M. In-situ HRTEM studies of alumina-aluminium solid-liquid interfaces. *Korean J. Electron Microsc. Spec. Issue* **2006**, *1*, 19–24.
26. Kauffmann, Y.; Oh, S.H.; Koch, C.T.; Hashibon, A.; Scheu, C.; Rühe, M.; Kaplan, W.D. Quantitative analysis of layering and in-plane ordering at an alumina-aluminum solid-liquid interface. *Acta Mater.* **2011**, *59*, 4378–4386.
27. Men, H.; Fan, Z. Prenucleation induced by crystalline substrates. *Metall. Mater. Trans. A* **2018**, *49*, 2766–2777.
28. Hashibon, A.; Adler, J.; Finnis, M.W.; Kaplan, W.D. Ordering at solid-liquid interfaces between dissimilar materials. *Interface Sci.* **2001**, *9*, 175–181.
29. Hashibon, A.; Adler, J.; Finnis, M.W.; Kaplan, W.D. Atomistic study of structural correlations at a liquid-solid interface. *Comput. Mater. Sci.* **2002**, *24*, 443–452.
30. Men, H.; Fan, Z. Atomic ordering in liquid aluminium induced by substrates with misfits. *Comput. Mater. Sci.* **2014**, *85*, 1–7.
31. Geysermans, P.; Gorse, D.; Pontikis, V. Molecular dynamics study of the solid-liquid interface. *J. Chem. Phys.* **2000**, *113*, 6382–6389.
32. Jiang, B.; Men, H.; Fan, Z. Atomic ordering in the liquid adjacent to an atomically rough solid surface. *Comput. Mater. Sci.* **2018**, *153*, 73–81.
33. Fang, C.M.; Men, H.; Fan, Z. Effect of substrate chemistry on prenucleation. *Metall. Mater. Trans. A* **2018**, *49*, 6231–6242.
34. Fan, Z. An epitaxial model for heterogeneous nucleation on potent substrates. *Metall. Mater. Trans. A* **2013**, *44*, 1409–1418.
35. Fan, Z.; Men, H.; Wang, Y.; Que, Z.P. A new atomistic mechanism for heterogeneous nucleation: Creating a 2D template for crystal growth. *Metals* **2021**, *11*, 478.
36. Fan, Z.; Men, H. A molecular dynamics study of heterogeneous nucleation in generic liquid/substrate systems with positive lattice misfit. *Mater. Res. Express* **2020**, *7*, 126501.
37. Hoyt, J.J.; Garvin, J.W.; Webb III, E.B.; Asta, M. An embedded atom method interatomic potential for the Cu-Pb system. *Model. Simul. Mater. Sci. Eng.* **2003**, *11*, 287–299.
38. Webb III, E.B.; Grest, G.S.; Heine, D.R. Precursor film controlled wetting of Pb on Cu. *Phys. Rev. Lett.* **2003**, *91*, 236102.
39. Hoyt, J.J. Molecular dynamics study of equilibrium concentration profiles and the gradient energy coefficient in Cu-Pb nanodroplets. *Phys. Rev. B* **2007**, *76*, 094102.
40. Kim, W.T.; Cantor, B. Solidification behaviour of Pb droplets embedded in a Cu matrix. *Acta Metall. Mater.* **1992**, *40*, 3339–3347.
41. Bilalbegovic, G.; Ercolessi, misfit.; Tosatti, E. Orientational phase separation for vicinal surfaces close to the nonmelting Pb(111) face. *Europhys. Lett.* **1992**, *17*, 333–337.
42. Bolcavage, A.; Kao, C.R.; Chen, S.-L.; Chang, Y.A. Thermodynamic calculation of phase stability between copper and lead-indium solder. In *Applications of Thermodynamics in Synthesis and Processing of Materials*; Nash, P., Sundman, B., Eds.; TMS: Warrendale, PA, USA, 1995.
43. Plimpton, S. Fast parallel algorithms for short-range molecular dynamics. *J. Comput. Phys.* **1995**, *117*, 1–19.
44. Hook, J.R.; Hall, H.E. *Solid State Physics*, 2nd ed.; Wiley: Chichester, UK, 1991.
45. Thompson, A.P.; Plimpton, S.J.; Mattson, W. General formulation of pressure and stress tensor for arbitrary many-body interaction potentials under periodic boundary conditions. *J. Chem. Phys.* **2009**, *131*, 154107.
46. Steinhardt, P.J.; Nelson, D.R.; Ronchetti, M. Bond-orientational order in liquids and glasses. *Phys. Rev. B* **1983**, *28*, 784–805.
47. Grimmer, H.; Bollmann, W.; Warrington, D.H. Coincidence-site lattices and complete pattern-shift in cubic crystals. *Acta Crystallogra. A* **1974**, *30*, 197–207.
48. Men, H.; Fan, Z. The study on prenucleation and heterogeneous nucleation in liquid Pb on solid Al with MD simulation. Brunel Centre for Advanced Solidification Technology (BCAST), Brunel University London, Uxbridge, UK. 2022, *to be submitted*.
49. Fan, Z.; Men, H. An overview on atomistic mechanisms of heterogeneous nucleation. *Metals* **2022,** *12*, 1547.
50. Ranganathan, S. On the geometry of coincidence-site lattices. *Acta Cryst.* **1966**, *21*, 197–199.
51. Kelton, K.F.; Greer, A.L. *Nucleation in Condensed Mater: Applications in Materials and Biology*; Elsevier Science: Oxford, UK, 2010.
52. Fan, Z.; Gao, misfit.; Jiang, B.; Que, Z.P. Impeding nucleation for more significant grain refinement. *Sci. Rep.* **2020**, *10*, 9448.
53. Quested, T.E. Understanding mechanisms of grain refinement of Al alloys by inoculation. *Mater. Sci. Technol.* **2004**, *20*, 1357–1369.